Plastic faulting: Brittle-like failure under high confinement

Carl E. Renshaw
Department of Earth Sciences, Dartmouth College, Hanover, New Hampshire, USA

Erland M. Schulson
Thayer School of Engineering, Dartmouth College, Hanover, New Hampshire, USA

Received 17 December 2003; revised 8 June 2004; accepted 8 July 2004; published 28 September 2004.

[1] Two distinct modes of compressive brittle-like failure are observed in laboratory samples of rock and ice. Under low to moderate confinement, terminal failure follows microcrack growth and interaction when damage is localized along a fault oriented $\sim$30° to the greatest compressive stress. Under higher confinement, frictional sliding is suppressed, and sudden, localized, brittle-like failure is not attended by a concentration of microcracks near the main fault. Also, faults that form under higher confinement are narrower and oriented $\sim$45° to the greatest compressive stress. We propose that these more steeply inclined faults are plastic faults whereby deformation is localized because of an instability that develops when thermal softening exceeds strain hardening. Analysis leads to a quantitative model for the shear stresses required to initiate and maintain the instability and to accommodate slip along the fault. The required stress is in general agreement with observed failure stresses from a variety of crystalline materials. Application of this model suggests that in some cases plasticity, rather than friction, limits the strength of the Earth's upper crust. *INDEX TERMS:* 5120 Physical Properties of Rocks: Plasticity, diffusion, and creep; 5104 Physical Properties of Rocks: Fracture and flow; 3902 Mineral Physics: Creep and deformation; 3924 Mineral Physics: High-pressure behavior; 3210 Mathematical Geophysics: Modeling; *KEYWORDS:* fracture, plasticity, creep, adiabatic shear, high confinement

Citation: Renshaw, C. E., and E. M. Schulson (2004), Plastic faulting: Brittle-like failure under high confinement, *J. Geophys. Res.*, *109*, B09207, doi:10.1029/2003JB002945.

1. Introduction

[2] In experimental studies of rock and ice loaded under compression, two distinct modes of sudden, brittle-like failure are observed. Under low to moderate confinement similar to conditions in the upper crust of the Earth, failure begins when microcracks initiate and slide [*Ashby and Hallam*, 1986; *Brace and Bombolakis*, 1963; *Horii and Nemat-Nasser*, 1986]. Terminal failure follows crack growth and interaction and is accompanied by a rapid increase in acoustic emission as damage is localized along a fault oriented at an angle $\theta_o \sim 30°$ to the greatest compressive stress, σ_1 [*Lockner et al.*, 1991; *Renshaw and Schulson*, 2001; *Shimada*, 1992]. The strength [*Byerlee*, 1978] and orientation of these faults are consistent with the dictates of Mohr-Coulomb friction. Accordingly, the angle θ_o only depends on the coefficient of friction, μ, as $\theta_o = 45° - 0.5° \tan^{-1}\mu$ [*Jaeger and Cook*, 1979]. Laboratory-derived values of μ (0.5–0.9) [*Byerlee*, 1978; *Kennedy et al.*, 2000] imply $\theta_o = 24°–32°$, in general agreement with both laboratory observations and the most commonly observed reverse fault orientations in the field [*Sibson and Xie*, 1998]. We term this type of failure Coulombic (C) faulting. The well-established mechanics of C faulting clearly require that confinement must be sufficiently low to allow frictional sliding along microcracks [*Renshaw and Schulson*, 2001; *Schulson*, 2002].

[3] Under the higher confinement that exists deeper in the Earth's crust, frictional sliding is suppressed, but brittle-like (i.e., sudden, localized) failure may still occur. In laboratory experiments, the characteristics of faults that form under confinement sufficient to suppress C faulting are distinctly different from those described above. Brittle-like compressive failure under high confinement is not attended by a significant increase in acoustic emission before failure, nor by a concentration of microcracks near the main fault [*Shimada*, 1992]. Also, faults that form under high confinement are narrower than C faults and, most significantly, are oriented close to the plane of maximum shear stress (θ_o = 45°) in both ice [*Schulson*, 2002] and rock [*Hirth and Tullis*, 1994; *Shimada*, 1992; *Tullis and Yund*, 1977].

[4] Observations of brittle-like failure under confinement sufficient to suppress frictional sliding imply the existence of an alternative, non-Coulombic faulting mechanism [*Evans et al.*, 1990]. Whereas Coulombic faulting at both the macroscopic [*Anderson*, 1972] and, more recently, the micromechanical [*Ashby and Hallam*, 1986; *Renshaw and Schulson*, 2001] level is well understood, the nature of brittle-like failure under higher confinement is an open question [*Evans et al.*, 1990].

0148-0227/04/2003JB002945$09.00

[5] In this paper we propose that in some cases brittle-like failure under high confinement may be driven by plastic (P) faulting whereby deformation is localized by an instability that develops within a shear zone when thermal softening exceeds strain hardening [*Hobbs et al.*, 1986; *Orowan*, 1960; *Schulson*, 2002]. Analysis of this mechanism leads to quantitative models for the shear stress required to both initiate and maintain plastic faulting. We demonstrate that the shear stress required to maintain plastic faulting is similar to the terminal failure strengths of a variety of crystalline materials in which plastic faulting is observed, thereby providing quantitative support for our model.

2. Confinement Versus Failure Mode

[6] To demonstrate that an alternative failure mode occurs when frictional sliding is suppressed, in Figure 1 we plot the morphologic style of faulting observed in laboratory specimens of rock and ice as a function of the confinement, or stress ratio $R = \sigma_3/\sigma_1$ (where σ_1 and σ_3 are the most and the least compressive stresses, respectively) versus the ratio of temperature-enhanced relaxation to strain hardening at failure (discussed in section 3). Non-Coulombic style faults (open symbols) were identified primarily by their orientation ($\sim 45 \pm 5^\circ$ to σ_1) and, when available, by their acoustic emission signature, by their narrow width, and/or by the low concentration of microcracks near the main fault. For a variety of crystalline materials in which both Coulombic and non-Coulombic style faults have been observed, the transition from one failure mode to the other is in good agreement with the confinement ratio required to suppress frictional sliding, R_c, given by [*Ashby and Hallam*, 1986]

$$R_c \equiv \frac{\sigma_3}{\sigma_1} > \frac{(1+\mu^2)^{0.5} - \mu}{(1+\mu^2)^{0.5} + \mu}. \quad (1)$$

That this criterion marks the upper limit for the transition from C faulting to another failure mode was recently established for ice [*Schulson*, 2002].

[7] What underlies this transition to non-Coulombic faulting? Of the mechanisms that have been proposed to explain non-Coulombic failure in relation to deep focus earthquakes, most do not seem to account for the high-confinement behavior shown in Figure 1. The data shown in Figure 1 were obtained from samples that were all initially dry, implying that faulting was not assisted by high pore pressures [*Hubbert and Rubey*, 1959]. Also, the rock types are not rich in hydrated mineral phases nor are the failure stresses (mean stresses generally $\sim$1 GPa or less) consistent with the pressures required for dehydration reactions (e.g., 2–9 GPa for the dehydration of serpentinite [*Meade and Jeanloz*, 1991]). Also, while the characteristics of the high-confinement faults shown in Figure 1 (i.e., narrow widths and orientations close to the plane of maximum shear stress) are similar to those associated with transformational faulting [*Kirby*, 1987], the observed failure stresses are again too low. For example, the mean stresses at failure for the ice data in Figure 1 are in the range 10–20 MPa, while the stress required to activate the polymorphic phase change from ice Ih to ice II occurs at a mean stress in the range 100–200 MPa [*Kirby*, 1987]. Similarly, the mean stresses for the transformational phase changes in rocks thought to be associated with deep focus earthquakes (e.g., olivine $\rightarrow$ spinel, tremolite $\rightarrow$ diopside [*Kirby*, 1987]) are generally greater than the failure stresses for the materials noted in Figure 1.

[8] In recognition of similar localized failures which develop in metals [*Basinski*, 1957], polymers [*Winter*, 1975] and metallic glasses [*Chen*, 1973; *Perez-Prado et al.*, 2001], we suggest that in some cases non-Coulombic faulting may be driven by adiabatic shear. The idea is that localization sets in when thermal softening exceeds strain hardening [*Hobbs et al.*, 1986; *Orowan*, 1960; *Schulson*, 2002]. We term this style plastic or P faulting, and outline below a model of the process. Adiabatic shear, we note, has been invoked previously to explain some deep focus earthquakes [*Branlund et al.*, 2000; *Griggs and Baker*, 1969; *Hobbs and Ord*, 1988; *Karato et al.*, 2001; *Ogawa*, 1987; *Wiens*, 2001]. In modeling this phenomenon, however, the existing theory is incomplete (more below).

3. Plastic Instability Criterion

[9] During failure under low to moderate confinement, several recent models have demonstrated that heating associated with sliding along shear faults can reduce frictional resistance [*Andrews*, 2002; *Garagash and Rudnicki*, 2003; *Lachenbruch*, 1980; *Mase and Smith*, 1987; *Raleigh and Evernden*, 1981; *Shaw*, 1995; *Sleep*, 1995]. Under confinement sufficient to suppress Coulombic failure, similar shear heating may result in a plastic instability when the increase in temperature resulting from shear deformation along the fault plane is so large that thermal softening exceeds both strain and strain rate hardening. The necessary condition for a plastic instability can be approximated by [*Hobbs et al.*, 1986]

$$\frac{\partial \tau}{\partial \gamma} < \frac{\tau^2 Q k}{nRT^2 c\rho}, \quad (2)$$

where τ and γ are shear stress and strain, respectively, c is the specific heat, ρ is the density, k is the fraction of heat retained in the deforming region, Q is the activation energy for creep, T is the temperature, R is the gas constant, and n is the stress exponent in the power law creep equation $\partial\gamma/\partial t = Ae^{-Q/(RT)}(\sigma_1 - \sigma_3)^n$, where A is a material constant and t is time. We estimate the strain hardening term (left-hand side of equation (2)) from expressions for transient creep which lead to a relationship of the form [*Hobbs et al.*, 1986]

$$\frac{\partial \tau}{\partial \gamma} \approx \lambda \tau, \quad (3)$$

where the parameter λ is of the order 10^{-1}–10^{0} [*Hobbs and Ord*, 1988]. In reviewing experiments in which terminal failure was non-Coulombic, we find upon inserting experimental measurements (using $\tau = \tau_o = (\sigma_1 - \sigma_3)/2$ at terminal failure) that the ratio of thermal softening to strain hardening (i.e., right-hand side of equation (2) divided by right-hand side of equation (3)) exceeds unity when we take $k = 1$ and adopt a midrange value $\lambda = 0.3$ (Figure 1). Table 1 lists appropriate parametric values. The non-Coulombic style faults shown in Figure 1 thus occur under

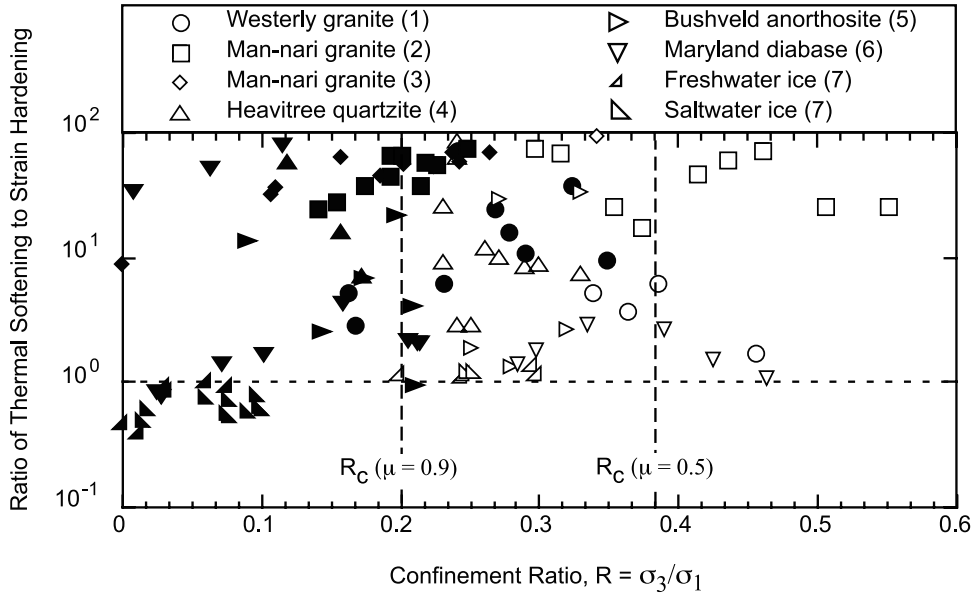

Figure 1. Morphologic style of brittle-like compressive failure as a function of the ratio of thermal softening to strain hardening at failure and the confinement ratio for a variety of crystalline materials in which both Coulombic (solid symbols) and non-Coulombic (open symbols) faulting have been observed. Thermal softening exceeds strain hardening in region above the horizontal dashed line. Vertical dashed lines indicate confinement ratio at which frictional sliding is suppressed for the indicated value of the coefficient of friction. References indicated by numbers in parentheses are as follows: (1) *Tullis and Yund* [1977], (2) *Shimada* [1992], (3) *Shimada and Cho* [1990], (4) *Hirth and Tullis* [1994], (5) *Tullis and Yund* [1992], (6) *Caristan* [1982], (7) *Schulson and Gratz* [1999].

conditions that are consistent with the existence of adiabatic shear instabilities.

4. Driving Stress

[10] Equation (2) defines a necessary, but not sufficient, condition for P faulting. This is demonstrated in Figure 1 which shows that the ratio of thermal softening to strain hardening at plastic failure can vary over more than 2 orders of magnitude. In addition to the instability criterion, the applied shear stress must be sufficient to both initiate and maintain localized deformation along the fault plane. We develop below (section 5) a quantitative model for the initiation of P faults. However, first we determine the stress required to maintain localized deformation and show it to be in good agreement with the terminal failure strengths when failure is non-Coulombic. Our approach is as follows. First, we seek expressions for the critical strain and strain rate required to maintain localized deformation along a P fault [*Frost and Ashby*, 1982]. We then combine the critical strain and strain rate with an expression for the power law creep of the material within a plastic fault shear zone that has been adiabatically heated.

[11] We propose that localized deformation along a plastic fault will be maintained when the shear strain rate within the plastic fault shear zone is sufficient to maintain adiabatic conditions ($k \sim 1$). We recognize that thermal softening instabilities can occur even when there is heat loss from the shear zone ($k < 1$). However, if the strain rate within the shear zone is significantly lower than that required for adiabatic conditions, then the loss of heat from the shear zone will be too great for thermal softening to overcome strain hardening and an instability will not develop (equation (2)). Conversely, higher strain rates require greater stress. Thus the minimum stress required to maintain plastic faulting can be approximated from the strain rate just sufficient to maintain adiabatic conditions.

[12] The shear strain rate within the shear zone that is just sufficient to maintain adiabatic conditions can be estimated

Table 1. Rock and Ice Parameters[a]

Rock	r_c, cm	Log A, MPa^{-n} s^{-1}	Q, kJ mol^{-1}	Source for A and Q
Dry Westerly granite	0.3	−5.7	187	*Carter and Tsenn* [1987]
Wet Westerly granite	10[b]	−3.7	141	*Carter and Tsenn* [1987]
Man-nari granite	0.4	−5.7	200	estimated based on Westerly granite
Heavitree quartzite	0.3	−9.4	99	fit to data from *Hirth and Tullis* [1994]
Bushveld anorthosite	0.3	−10.5	58	fit to data from *Tullis and Yund* [1992]
Maryland diabase	0.6	−1.2	276	*Carter and Tsenn* [1987]
Ice[b]	7.7	6.5	70	*Sanderson* [1988]

[a]For all materials, $n = 3$, $\rho = 2650$ kg m^{-3}, $c = 10^3$ J kg^{-1} K^{-1} except for dry Westerly and Man-nari granite, $n = 3.3$; for wet Westerly granite, $n = 1.9$; and for ice, $\rho = 920$ kg m^{-3}, $c = 1280$ J kg^{-1}K^{-1}.

[b]The effect of porosity on the creep of saltwater ice is neglected. See discussion by *Sanderson* [1988].

from the critical shear strain required for localization, $\gamma_c = m\sigma_c/(\partial\tau_o/\partial T)$, and from the characteristic thermal diffusion time [*Frost and Ashby*, 1982]. Accordingly, the local strain rate within the shear zone is given by

$$\left(\frac{\partial\gamma}{\partial t}\right)_c \approx \frac{2\gamma_c\alpha\kappa}{\rho c r_c^2} = \frac{-m\kappa}{(\partial\tau_o/\partial T)r_c^2}, \tag{4}$$

where α is a constant of order 10^0, κ is the thermal conductivity, r_c is a characteristic dimension (e.g., the radius of a cylindrical sample), and m is the work-hardening exponent in the power law stress-strain relationship $\tau_o = \beta\gamma^m$, where β is a constant. The corresponding global strain rate is obtained by multiplying the local strain rate by $L_z/(2L)$, where L is the length of the specimen and L_z is the width of the shear zone.

[13] Upon equating the global strain rate to the power law creep expression and assuming deformation occurs along the plane of maximum shear stress ($\theta_o = 45°$), we thus estimate the shear stress, τ_m, required to maintain P faulting by the relationship

$$\tau_m \approx \frac{1}{2}\left[\frac{-m\kappa L_z}{2L(\partial\tau_o/\partial T)r_c^2 A e^{-Q/(RT)}}\right]^{1/n}. \tag{5}$$

In Figure 2a we compare the shear stress given by equation (5) to the imposed shear stress at terminal failure, τ_o, of rock when failure is non-Coulombic. In making these calculations we used the values listed in Table 1 for r_c, A, and Q; assumed that $m = 0.3$; and used $\kappa \sim 2$ W (mK)$^{-1}$. We obtained the thermal softening term $\partial\tau_o/\partial T \sim -0.8$ MPa K^{-1} from a least squares linear fit to a plot of temperature versus the compressive strength of granitic rock when failure was non-Coulombic (Figure 3). We estimated $L_z \sim 10^{-4}$ m from photomicrographs of plastic faults in quartzite [*Hirth and Tullis*, 1994]. While the estimated shear stress required to maintain P faulting is similar to the terminal failure stress for samples deformed at high temperatures (Figure 2a), the estimated shear stress is orders of magnitude greater than the measured failure stress at lower temperatures. In fact, the measured terminal failure stress is only weakly dependent upon temperature. We propose therefore that the appropriate temperature for estimating the required shear stress is not the ambient temperature at which the sample was deformed, but rather the temperature of the material within the shear zone.

[14] No direct measurements exist of the temperature along a P fault. However, a first approximation suggests significant heating, consistent with the fact that greater than 90% of the energy associated with plastic deformation is converted to heat [*Dieter*, 1986], at least in metals. If we assume that all the work in creating a shear zone is converted to heat, then the increase in temperature within the newly created shear zone is given by [*Frost and Ashby*, 1982; *Rubin and Drucker*, 1969]

$$\Delta T = \frac{\tau_o\gamma_c}{\rho c} = -\frac{m\tau_o}{2(\partial\tau_o/\partial T)}. \tag{6}$$

Typical terminal failure strengths are of the order 10^1 MPa for ice at -10°C and 10^3 MPa for rock at temperatures up to $\sim$1000°C, leading to typical increases in temperature of several degrees for ice (using $\partial\tau_o/\partial T \sim -0.4$ MPa K^{-1} [*Schulson*, 2002]) and of several hundred degrees for rock. Additional heating will occur as further shear accommodates the continued propagation of the fault. The predicted temperature increase is consistent with observations of recrystallization and melting in ice between -10°C and -1°C undergoing simple shear [*Burg et al.*, 1986; *Wilson et al.*, 1996].

[15] The temperature increase in the shear zone is bounded by the melting temperature, for as the temperature approaches this point the shear strength decreases, reducing the production of additional heat. Temperatures along P faults near the melting point are consistent with microstructural observations of recrystallized grains within P faults in ice [*Meglis et al.*, 1999; *Schulson and Gratz*, 1999]. Evidence for recrystallization along P faults in rock is inconclusive, partially due to the extremely narrow nature of P faults and, perhaps, partially due to the complexity of the melting process in polymineralic material. However, field studies have documented high dislocation densities, recrystallized quartz grains, and other microstructural evidence that is indicative of thermally activated plasticity within faults [see *Hirth and Tullis*, 1994].

[16] It might be argued that at temperatures near the melting temperature the dominant deformation mechanism becomes a viscous process such as diffusion creep ($n \sim 1$) rather than the dislocation creep ($n \sim 3$) that we invoked above. However, experimental observations of creep rates in ice near its melting temperature (-2°C) indicate a creep law exponent $n \sim 3$ (and not $n \sim 1$) [*Barnes et al.*, 1971], consistent with our assumption of dislocation creep. Similarly, observations of recrystallization and high dislocation densities [see *Hirth and Tullis*, 1994] along faults formed in rock under high confinement are consistent with dislocation creep as the dominant deformation mechanism.

[17] Taking, then, the melting temperature as an upper bound estimate of the temperature within the shear zone, Figure 2b compares the imposed shear stress required to maintain slip along the fault plane via thermal softening to observed terminal failure strengths in rock and ice. Parametric values are the same as given above with the addition of $\kappa \sim 8$ W (mK)$^{-1}$ for ice and of $L_z \sim 10^{-2}$ mm for ice based on photomicrographs of plastic faults in ice [*Iliescu*, 2000]. The grayed region indicates the range of uncertainty for the stress required to maintain plastic faulting assuming that m and $\partial\tau_o/\partial T$ are within a factor of 3 of the value we estimated. In general, there appears to be quite good correspondence between the stresses we calculate to maintain plastic faulting and the measured terminal failure strengths under high confinement.

5. Plastic Fault Initiation

[18] The analysis above demonstrates that once a plastic fault localizes, propagation of the fault can generate sufficient heat to maintain localized deformation along the growing fault plane in an autocatalytic manner. To initiate this process, however, it is necessary to both localize deformation and to raise the temperature of the material in the incipient fault region sufficiently to start the auto-

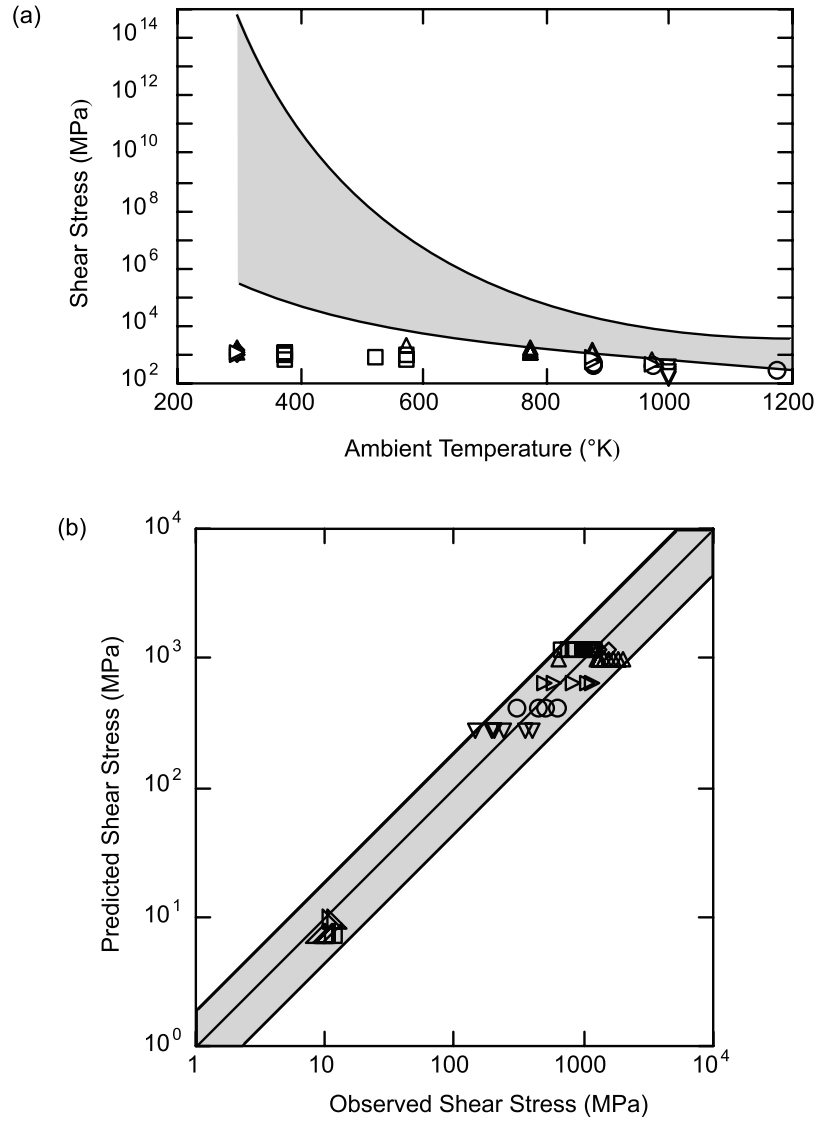

Figure 2. (a) Shear stress at failure versus ambient temperature in rock samples where failure was non-Coulombic. Shaded region indicates range of shear stresses required to maintain a plastic instability predicted by equation (5) using the ambient temperature and the rock properties listed in Table 1. (b) Observed shear stress at non-Coulombic failure versus the shear stress required to maintain a plastic instability predicted by equation (5) using the temperature at which the material completely melts. Here we approximate this upper limit as 1000°C for rock and use 0°C for ice. Shaded region indicates range of uncertainty for plastic faulting assuming m and $\partial\tau_o/\partial T$ are both correct to within a factor of 3. Symbols and data sources are the same as in Figure 1. All rocks were deformed at a strain rate of 10^{-5} or 10^{-6} s^{-1}, except for two samples of Maryland diabase deformed 10^{-3} s^{-1}. All ice samples were deformed at a strain rate of 6×10^{-3} s^{-1}.

catalytic process. In the discussion below we propose one possible mechanism by which this may occur.

[19] As already noted, microstructural analyses of rock clearly demonstrate the strong association between plastic faults and dislocations. For instance, dislocation densities in grains directly adjacent to plastic faults can be as high as $\sim 10^{15}$ m^{-2} [*Hirth and Tullis*, 1994]. In the early stages of plastic deformation, experiment and theory suggest that grain boundaries are the dominant source of dislocations [*Li*, 1963; *Liu et al.*, 1992]. Once created, these dislocations may glide across the grain and begin to pile up at a grain boundary [*Baker et al.*, 1986; *Liu et al.*, 1995; *Dieter*, 1986]. Multiple dislocation sources may be present along a single grain boundary, creating a series of closely spaced pileups that may interact to initiate the plastic fault. For simplicity, however, we only consider a single pileup. For a grain of diameter d, the number of dislocations n_d in a single pileup is given by [*Eshelby et al.*, 1951]

$$n_d = \frac{f\pi\tau_s d}{4Gb}, \tag{7}$$

where τ_s is the average resolved shear stress in the slip plane, G is the shear modulus, b is the Burgers' vector of the

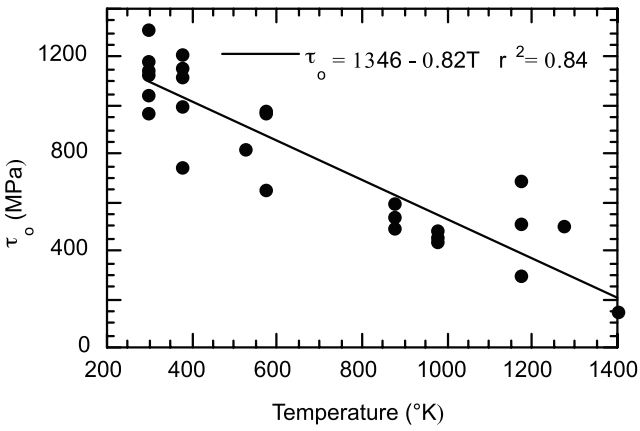

Figure 3. Plastic compressive strength versus temperature for granitic rock. Least squares linear fit to the data yields $\partial\tau_o/\partial T \sim -0.8$ MPa K^{-1}. Data are from *Shelton et al.* [1981], *Shimada* [1992], *Shimada and Cho* [1990], *Tullis and Yund* [1992], and *Tullis and Yund* [1977]. Data were generated from tests at strain rates of $10^{-6} - 10^{-5}$ s^{-1}.

dislocations, and f is a factor close to unity. The total offset across the slip plane is simply $n_d b$.

[20] If the applied shear stress continues to increase, then at a critical stress slip will propagate across the grain boundary barrier. If the propagation across the barrier occurs quickly, then this is essentially an adiabatic process. In this case, as before (equation (6)), the increase in temperature, ΔT, can be approximated as

$$\Delta T = \frac{\tau_s \gamma}{\rho c}, \tag{8}$$

where the shear strain γ is defined as $n_d b/(2L_o)$, where L_o is the width of the slip band.

[21] Photomicrographs of dislocation pile ups at grain boundaries in alloys suggest that typical shear bandwidths, L_o, are on the order of several tenths of a micrometer [e.g., *Baker et al.*, 1986]. Similar data are not available for rocks, but *Hirth and Tullis* [1994] have observed fully developed plastic faults that are less than a micrometer wide, suggesting that L_o in rocks may also be of the order of a fraction of a micrometer. Using the conservative estimate $L_o = 10^{-6}$ m, the estimated shear strain associated with the propagation of slip across the grain boundary barrier $\gamma = n_d b/(2L_o)$ is greater than γ_c, the minimum shear strain required for shear strain localization in both rock and ice (equation (4)).

[22] The resolved shear stress τ_s is related to the applied shear stress τ as

$$\tau_s = \tau - \tau_i, \tag{9}$$

where τ_i is the friction stress required to overcome lattice resistance to dislocation motion, i.e., the Peierls stress. Although this term is poorly constrained for rock, for quartz and many silicon and aluminum oxides, τ_i is generally about $10^{-2}G$ [*Frost and Ashby*, 1982]. For rock, $G \sim 10$ GPa, suggesting that τ_i is about one tenth to one half of the terminal failure stress for plastic faulting (Figure 2). Similarly, measurements in ice at 253–268 K yield $\tau_i \sim 1$ MPa [*Schulson et al.*, 1984], or about one tenth of the terminal failure stress for plastic faulting at these temperatures. Taking $\tau_o = (\sigma_1 - \sigma_3)/2$ at terminal failure and conservatively assuming $\tau_i = 0.5\tau_o$, the predicted increase in temperature associated with the propagation of slip across the grain boundary barrier are several degrees for ice and several hundred degrees for rock. In this calculation we set $G = 3.5$ GPa for ice [*Gammon et al.*, 1983] and assume $d = 10^{-3}$ m and $d = 10^{-2}$ m for rock and ice, respectively.

[23] We thus conclude that both the shear strain and the increase in temperature associated with the breakthrough of dislocation slip across grain boundaries are sufficient to initiate plastic faults. Once initiated, the newly formed plastic fault will continue to propagate as long as the applied shear stress is sufficient to maintain localized deformation, as discussed above.

6. Can Plastic Faults Initiate in the Uppermost Crust?

[24] Implicit in the above model for the initiation of plastic faults is the existence of dislocation pileups. This requires that the combination of strain rate and temperature be sufficient for the creation and glide of a large number of dislocations (e.g., see equation (7)). Consequently, we do not expect dislocation pileups to form, nor plastic faulting to occur, within the uppermost brittle field of the crust where creep processes are not sufficiently active.

[25] To quantify this idea, we consider the time required for a dislocation to move across a grain and compare this to the time required for a typical geologic strain rate to generate stress within the brittle crust sufficient to induce brittle failure. While dislocation velocities in rock are poorly constrained, *Krausz* [1970] argues that dislocation velocity can be described in terms of physical concepts by using a reaction rate theory model of the asymmetrical energy barrier to dislocation movement and assuming that the activation energy of the rate controlling process is linearly dependent on the resolved shear stress. The resulting expression for the dislocation velocity, v, can be written

$$v = \Omega_f \exp\left(-\frac{\Psi_f - V_f\tau}{KT}\right) - \Omega_b \exp\left(-\frac{\Psi_b + V_b\tau}{KT}\right), \tag{10}$$

where Ω is a constant related to the transmission coefficient for the activation of a dislocation, Ψ is the activation energy for dislocation movement, V is the activation volume, τ is the resolved shear stress acting on the dislocation, and K is the Boltzmann constant. The subscripts f and b indicate the forward and backward movement of the dislocations across the possibly asymmetric energy barrier. *Krausz* [1970] states that this model describes well the dislocation velocities in a variety of semiconductors, metals, and ice.

[26] Given the dislocation velocity, the characteristic time for dislocation movement is given by

$$t_d = \frac{d}{v}. \tag{11a}$$

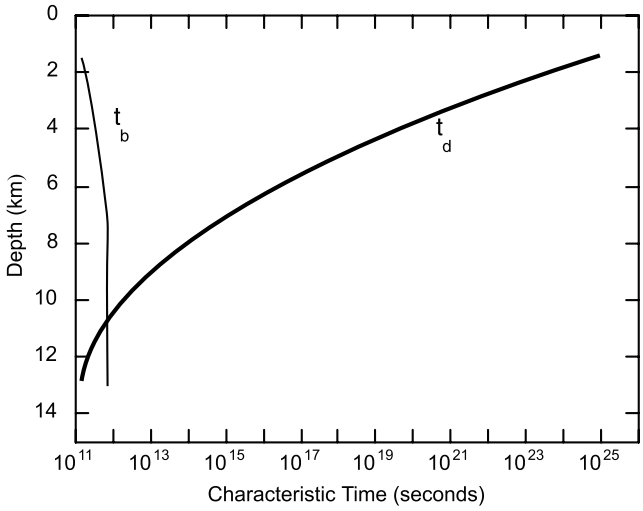

Figure 4. Characteristic times for dislocation movement across a grain and for brittle failure.

The corresponding characteristic time for brittle failure is given by

$$t_b = \frac{\tau_B}{G(d\gamma/dt)}, \tag{11b}$$

where τ_B is the brittle failure stress. Here we take τ_B as the C faulting failure stress for the formation of a reverse fault in a compressional environment where $\sigma_3 = \rho g z$, where z is depth. Coulombic faulting will occur when the excess shear stress exceeds the cohesive strength of the rock S_n [*Ashby and Hallam*, 1986]:

$$\frac{\sigma_1 - \sigma_3}{2} \sin 2\theta_o - \mu\left(\frac{\sigma_1 + \sigma_3}{2} \cos 2\theta_o - P\right) > S_n, \tag{12}$$

where P is the fluid pressure and θ_o again defines fault orientation (section 1). For the friction coefficient and cohesive strength, we used *Byerlee*'s [1978] values

$$\begin{array}{lll} \mu = 0.85; & S_n = 0 & \dfrac{\sigma_1 - \sigma_3}{2} \cos 2\theta_o - P < 200\,\text{MPa} \\ \mu = 0.6; & S_n = 80\,\text{MPa} & \text{otherwise.} \end{array} \tag{13}$$

Further assuming a typical geologic strain rate (10^{-13} s^{-1} [*Carter and Tsenn*, 1987]), the characteristic time for brittle failure t_b versus depth in the crust is shown in Figure 4.

[27] The necessary parametric values to estimate the characteristic time for dislocation movement in rock are not known. However, lacking more appropriate data, we demonstrate our approach by assuming that the values for rock are similar to those for Si. Thus the plot of τ_d versus depth for Si shown in Figure 4 may provide only an order of magnitude estimate of the characteristic time for dislocation movement in rock. In making this calculation, we assumed a typical crustal geothermal gradient (20° km^{-1} depth [*Carter and Tsenn*, 1987]), made the conservative assumption that the state of stress is defined by t_B, took $d = 10^{-3}$ m, and used for the parameters in equation (10) those given by *Krausz* [1970] for Si ($\Psi_f = 2.235$ eV, $\Psi_b = 2.215$ eV, $V_f = 71$ Å^3, $V_b = 31.5$ Å^3, and $\Omega_f = \Omega_b = 2 \times 10^8$ cm s^{-1}).

[28] Figure 4 shows that in the upper crust, dislocation movement is so slow that stresses increase to the brittle failure stress long before even a single dislocation can cross a typical grain. Thus it is not possible to create a dislocation pileup before C faulting occurs. However, deeper in the crust, dislocation velocity increases dramatically, such that for depths > ~11 km at a strain rate of 10^{-13} s^{-1}, the time required to create a dislocation pileup is similar to, or less than, that required for C faulting. While this conclusion is based on the assumption that dislocation velocities in rock are similar to those in Si, the difference in characteristic times shown in Figure 4 is so large (more than 10 orders of magnitude in the uppermost crust) that it is unlikely that a different parameterization would change the conclusion that dislocation velocity in the uppermost crust is too slow to permit the formation of dislocation pileups before C faulting occurs. Also, significantly, the transition from $t_b < t_p$ to $t_b > t_p$ occurs at the same depth as the transition from strength being limited by Byerlee's law to strength being limited by power law creep (see discussion of Figure 5). This provides post hoc support for using the

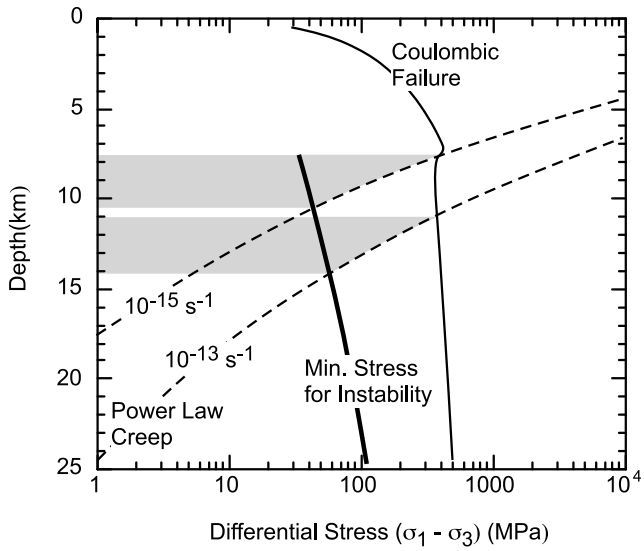

Figure 5. Differential stress as a function of depth for Coulombic failure as predicted by *Byerlee*'s [1978] law (solid line, equations (12) and (13)) and for steady power law creep as given by the power law creep expression $\partial\gamma/\partial t = Ae^{-Q/(RT)}(\sigma_1 - \sigma_3)^n$ for the indicated strain rate (dashed lines). Parametric values are those for wet Westerly granite (Table 1). Bold line shows minimum stress required for a thermal instability as given by equations (2) and (3). Upper and lower shaded regions show depths at which plastic faulting may occur for the slower and faster strain rates, respectively. These regions are defined by stresses sufficient for an adiabatic instability yet less than required for Coulombic failure.

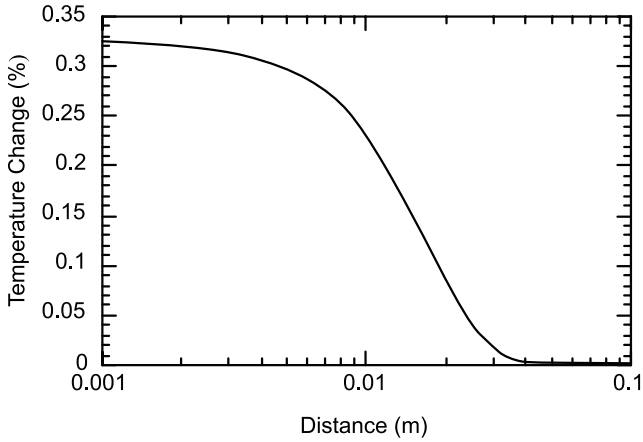

Figure 6. Temperature change $(T - T_o)/(T_f - T_o)$ as a function of distance from the fault zone after 100 s.

Si parameterization in the dislocation velocity model as an estimate of dislocation velocity in rock.

7. Implications to Failure of the Earth's Crust

[29] So far we have addressed deformation in the laboratory. The more important issue is: Do P faults occur in the Earth's crust? From a theoretical perspective we can begin to address this question by comparing the failure stress associated with plastic faulting with the failure stress associated with other mechanisms thought to be active in the Earth's crust.

[30] The rheology of the crust and lithosphere is usually described to first order using a simple, two-mechanism model in which the strength of the upper "brittle" crust is limited by frictional resistance (e.g., Coulombic faulting) while the strength of the lower crust is limited by creep. Specifically, the strength of the upper crust is given by *Byerlee*'s [1978] law, while at lower depths strength is assumed to be described by power law creep.

[31] In Figure 5 we plot, for a compressional environment, the differential failure stress $(\sigma_1 - \sigma_3)$ for wet Westerly granite as a function of depth in the crust, as predicted by both Byerlee's law and the power law creep expression. We assumed hydrostatic fluid pressure $P = \rho_w gz$, where ρ_w is the density of water. For power law creep we consider two geologically common crustal strain rates, $\partial\gamma/\partial t = 10^{-13}$ and $\partial\gamma/\partial t = 10^{-15}$ s^{-1} [*Carter and Tsenn*, 1987]. As expected, the minimum failure stress is governed by Coulombic failure in the upper crust. At a critical depth (here 11 and 7.5 km for strain rates of 10^{-13} and 10^{-15} s^{-1}, respectively) the creep rate becomes sufficient to prevent stresses from exceeding those required for Coulombic failure, suppressing the frictional failure mode. We do not expect plastic faulting to occur at depths less than these critical depths as the creep rate is likely too slow to create the necessary dislocation pileups before Coulombic failure occurs (section 6).

[32] Below these critical depths where the stress is governed by power law creep, plastic faulting may occur if the steady state creep stresses are sufficient to satisfy the instability criterion. The minimum stress satisfying this criterion, given by equation (2), is shown by the bold line in Figure 5. As indicated by the grayed regions in Figure 5, for several kilometers below the critical depth marking the suppression of Coulombic failure, the stresses predicted by the power law creep expressions are sufficient to satisfy the instability criterion.

[33] To estimate the actual plastic faulting failure stresses, we applied our model (equation (5)) to estimate the stress required to accommodate slip via thermal softening along a reverse fault dipping 45°. As before, we used the numerical values for wet Westerly granite. We set both of the characteristic dimensions, r_c and L, to be the distance over which heat can be conducted over the timescale of a typical large magnitude seismic event, and we obtained this distance as follows: Consider a fault zone in an infinite medium having an initially uniform temperature, T_o. If at time $t = 0$, adiabatic heating raises the temperature within the fault zone to T_f, then the variation in temperature over time t at distances r from the center of the fault zone is given by [*Carslaw and Jaeger*, 1959]

$$\frac{T - T_o}{T_f - T_o} = \frac{1}{2}\left[\operatorname{erf}\left(\frac{(L_z/2) + r}{2\sqrt{\kappa t/\rho c}}\right) + \operatorname{erf}\left(\frac{(L_z/2) - r}{2\sqrt{\kappa t/\rho c}}\right)\right]. \quad (14)$$

At the edge of the characteristic dimension, $T \approx T_o$ at time $t = t_s$, where t_s is the timescale of a typical large magnitude seismic event ($\sim 10^2$ s). On the basis of the microstructures of P faults in the laboratory samples, we set $L_z = 10^{-4}$m. We thus obtained the temperature as a function of distance, r (Figure 6). On the basis of Figure 6 we estimate $r_c = L = 0.04$ m. Using these numerical values, we obtained from equation (5) a shear stress of about 50 MPa to maintain localized plastic flow. This stress is similar to shear stresses inferred (~10–100 MPa) at midcrustal depth (5–15 km) [*Carter and Tsenn*, 1987; *Emmermann and Lauterjung*, 1997], suggesting that P faulting is possible at these depths. This stress is also similar to the minimum stress required for a thermal instability (equation (2)), suggesting that this necessary condition may be a good approximation of the plastic fault failure stress at these depths. We conclude that from a theoretical perspective plastic faulting is possible at midcrustal depths.

[34] Also consistent with the possibility of plastic faulting in the upper crust are the dips, θ_o of reverse faults associated with large ($M > 5.5$) intracontinental earthquakes [*Collettini and Sibson*, 2001]. While the primary peak in the distribution of dip angles (Figure 7a) is consistent with the dips expected from Coulombic faulting ($\theta_o = 24°–32°$ for $\mu = 0.5–0.9$ [*Anderson*, 1972]), a prominent secondary peak occurs at ~45° [*Sibson and Xie*, 1998].

[35] Several mechanisms have been proposed to explain the subsidiary peak in reverse fault orientations at $\theta_o \sim 45°$. For example, "domino steepening" of an initially low-angle thrust stack may occur in areas of intense shortening [*Sibson and Xie*, 1998]. However, in this case we would expect to find a broad distribution of orientations above the initial fault angle ($\theta_o \sim 30°$) representing the progressive steepening of faults with increased shortening. Instead, the distribution of orientations θ_o is bimodal. Alternatively, steeply dipping reverse faults may result from the compressional reactivation of former normal faults formed during an earlier phase of crustal extension [*Sibson and Xie*, 1998]. However,

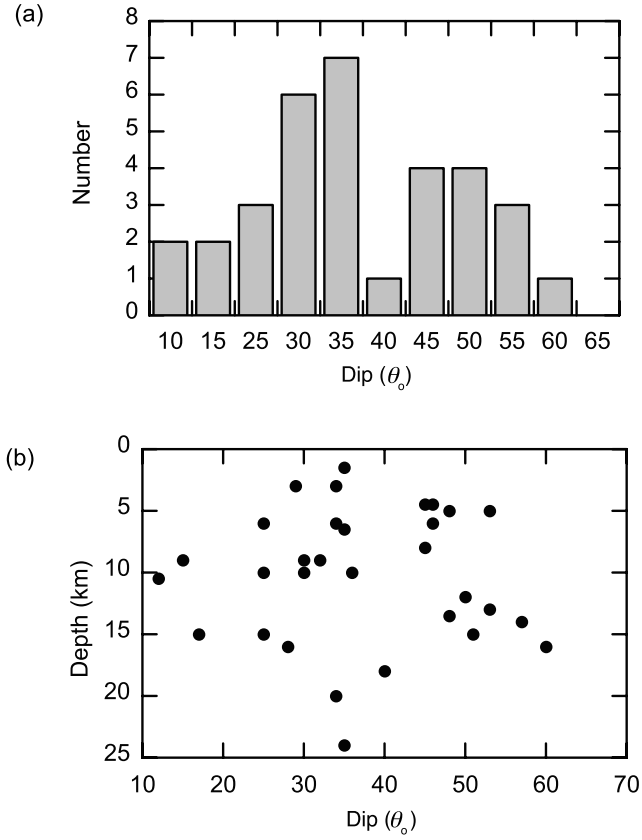

Figure 7. (a) Dip θ_o of reverse faults inferred from large magnitude ($M > 5.5$) earthquakes. Uncertainties in dip estimates are $\pm 5°-10°$. Replotted from *Collettini and Sibson* [2001]. (b) Reverse fault dip versus depth, as tabulated by *Sibson and Xie* [1998].

as noted by *Sibson and Xie* [1998], in addition to a tectonic inversion, the reactivation of the normal faults, rather than the creation of new favorably oriented reverse faults, requires substantial fluid overpressuring along the existing fault planes. In addition, it must be assumed that the fault has not healed during the possibly long interval over which the tectonic inversion occurs. A third explanation for steeply dipping reverse faults is a significant deviation of the greatest principal stress trajectory from the assumed horizontal orientation. This could be a consequence of, for example, horizontal ductile flow in the lower crust. In this case we would expect steeply dipping normal faults to be more common at greater depths. However, as shown in Figure 7b, there is no clear correlation between reverse fault dip and depth.

[36] While processes such as reactivation of normal faults probably explain many of the observed high-angle reverse faults, we note that seismically active conjugate strike-slip faults also tend to occur in orthogonal sets and can not be explained by reactivation [*Thatcher and Hill*, 1991]. Conjugate orthogonal sets of shear zones have also been documented in granite under greenschist (i.e., relatively low temperature and pressure) metamorphic conditions [*Mitra*, 1988]. Perhaps significantly, the dips of the high-angle reverse faults and the orthogonal sets of conjugate strike-slip faults are consistent with those expected if failure occurs via plastic faulting.

[37] We thus propose, based on their orientation and our analyses showing that the P faulting failure stress is similar to inferred stresses at midcrustal depths, that some steeply dipping reverse faults may represent P faults. We note that plastic faulting has been suggested previously as a possible mechanism for the generation of earthquakes in the deep crust [*Branlund et al.*, 2000; *Griggs and Baker*, 1969; *Hobbs and Ord*, 1988; *Karato et al.*, 2001; *Ogawa*, 1987; *Wiens*, 2001]. Our model supports the idea that plastic faulting may also occur in the semibrittle region at midcrustal depth, under stresses similar to those inferred at these depths. In these cases, plasticity, rather than friction, may limit strength when the confinement is sufficient to suppress Coulombic failure.

[38] **Acknowledgments.** We would like to thank the Associate Editor and the two anonymous reviewers for critical and helpful comments on an earlier version of this manuscript. This work was supported by the U.S. National Science Foundation (EAR-981412, OPP-0328605) and the National Oceanographic and Atmospheric Administration (NOAA-NA17RP1400).

References

Anderson, E. M. (1972), *The Dynamics of Faulting*, Hafner, Old Tappan, N. J.

Andrews, D. J. (2002), A fault constitutive relation accounting for thermal pressurization of pore fluid, *J. Geophys. Res.*, *107*(B12), 2363, doi:10.1029/2002JB001942.

Ashby, M. F., and S. D. Hallam (1986), The failure of brittle solids containing small cracks under compressive stress states, *Acta Metall.*, *34*(3), 497–510.

Baker, I., E. M. Schulson, and J. A. Horton (1986), Observation of slip propagation across grain boundaries in Ni_3Al, paper presented at 44th Annual Meeting, Electron Microsc. Soc. of Am., Albuquerque, N. M., 10–15 Aug.

Barnes, P., D. Tabor, and J. F. C. Walker (1971), The friction and creep of polycrystalline ice, *Proc. R. Soc. London*, *Ser. A*, *324*, 127–155.

Basinski, Z. S. (1957), The instability of plastic flow at very low temperatures, *Proc. R. Soc. London*, *Ser. A*, *240*, 229–242.

Brace, W. F., and E. G. Bombolakis (1963), A note on brittle crack growth in compression, *J. Geophys. Res.*, *68*, 3709–3713.

Branlund, J. M., M. Kameyama, D. A. Yuen, and Y. Kaneda (2000), Effects of temperature-dependent thermal diffusivity on shear instability in a viscoelastic zone: Implications for faster ductile faulting and earthquakes in the spinel stability field, *Earth Planet. Sci. Lett.*, *182*, 171–185.

Burg, J. P., C. J. L. Wilson, and J. C. Mitchell (1986), Dynamic recrystallization and fabric development during simple shear deformation of ice, *J. Struct. Geol.*, *8*(8), 857–870.

Byerlee, J. D. (1978), Friction of rocks, *Pure Appl. Geophys.*, *116*, 615–626.

Caristan, Y. (1982), The transition from high temperature creep to fracture in Maryland diabase, *J. Geophys. Res.*, *87*, 6781–6790.

Carslaw, H. S., and J. C. Jaeger (1959), *Conduction of Heat in Solids*, Oxford Univ. Press, New York.

Carter, N. L., and M. C. Tsenn (1987), Flow properties of continental lithosphere, *Tectonophysics*, *136*, 27–63.

Chen, H. S. (1973), Plastic flow in metallic glasses under compression, *Scr. Metall.*, *7*, 931–936.

Collettini, C., and R. H. Sibson (2001), Normal fault, normal friction?, *Geology*, *29*(10), 927–930.

Dieter, G. E. (1986), *Mechanical Mettallurgy*, 751 pp., McGraw-Hill, New York.

Emmermann, R., and J. Lauterjung (1997), The German Continental Deep Drilling Program KTB: Overview and major results, *J. Geophys. Res.*, *102*, 18,179–18,201.

Eshelby, J. D., F. C. Frank, and F. R. N. Nabarro (1951), The equilibrium of linear arrays of dislocations, *Philos. Mag.*, *42*(327), 351–364.

Evans, B., J. T. Fredrich, and T.-F. Wong (1990), The brittle-ductile transition in rocks: Recent experimental and theoretical progress, in *The Brittle-Ductile Transition in Rocks: The Heard Volume*, *Geophys. Monogr. Ser.*, vol. 56, edited by A. G. Duba et al. pp. 1–20, AGU, Washington, D. C.

Frost, H. J., and M. F. Ashby (1982), *Deformation-Mechanism Maps*, 121 pp., Permagon, New York.
Gammon, P. H., H. Kiefte, M. J. Clouter, and W. W. Denner (1983), Elastic constants of artificial ice and natural ice samples by brillouin spectroscopy, *J. Glaciol.*, *29*, 433–460.
Garagash, D. I., and J. W. Rudnicki (2003), Shear heating of a fluid-saturated slip weakening dilatant fault zone: 2. Quasi-drained regime, *J. Geophys. Res.*, *108*(B10), 2472, doi:10.1029/2002JB002218.
Griggs, D. T., and D. W. Baker (1969), The origin of deep focus earthquakes, in *Properties of Matter Under Unusual Condtions*, edited by H. Mark and S. Fernback, pp. 23–42, Wiley Interscience, Hoboken, N. J.
Hirth, G., and J. Tullis (1994), The brittle-plastic transition in experimentally deformed quartz aggregates, *J. Geophys. Res.*, *99*, 11,731–11,747.
Hobbs, B. E., and A. Ord (1988), Plastic instabilities: Implications for the origin of intermediate and deep focus earthquakes, *J. Geophys. Res.*, *93*, 10,521–10,540.
Hobbs, B. E., A. Ord, and C. Teyssier (1986), Earthquakes in the ductile regime?, *Pure Appl. Geoph.*, *124*(1/2), 309–336.
Horii, H., and S. Nemat-Nasser (1986), Brittle failure in compression: Splitting, faulting, and brittle-ductile transition, *Philos. Trans. R. Soc. London*, *Ser. A*, *319*, 337–374.
Hubbert, M. K., and W. W. Rubey (1959), Role of fluid pressures in mechanics of overthrust faulting: I, Mechanics of fluid-filled porous solids and its application to overthrust faulting, *Geol. Soc. Am. Bull.*, *70*, 115–166.
Iliescu, D. (2000), Contributions to brittle compressive failure of ice, Ph.D. thesis, Dartmouth Coll., Hanover, N. H.
Jaeger, J. G., and N. G. W. Cook (1979), *Fundamentals of Rock Mechanics*, 585 pp., Chapman and Hall, New York.
Karato, S., M. R. Riedel, and D. A. Yuen (2001), Rheological structure and deformation of subducted slabs in the mantle transition zone: Implications for mantle circulation and deep earthquakes, *Phys. Earth Planet. Inter.*, *127*, 83–108.
Kennedy, F. E., E. M. Schulson, and D. E. Jones (2000), The friction of ice on ice at low sliding velocities, *Philos. Mag.*, *80*, 1093–1110.
Kirby, S. H. (1987), Localized polymorphic phase transformations in high-pressure faults and applications to the physical mechanism of deep earthquakes, *J. Geophys. Res.*, *92*, 13,789–13,800.
Krausz, A. S. (1970), A rate theory analysis of the temperature dependence of dislocation velocity, *Mater. Sci. Eng.*, *6*, 260–264.
Lachenbruch, A. H. (1980), Frictional heating, fluid pressure, and the resistance to fault motion, *J. Geophys. Res.*, *85*, 6097–6112.
Li, J. C. M. (1963), Petch relation and grain boundary sources, *Trans. Metall. Soc. AIME*, *227*(1), 239–247.
Liu, F., I. Baker, G. Yao, and M. Dudley (1992), Dynamic observations of dislocation sources at grain boundaries in ice, *Philos. Mag. Lett.*, *65*, 279–281.
Liu, F., I. Baker, and M. Dudley (1995), Dislocation/grain boundary interactions in ice crystals, *Philos. Mag.*, *71*, 15–42.
Lockner, D. A., J. D. Byerlee, V. Kuksenko, A. Ponomarev, and A. Sidorin (1991), Quasi-static fault growth and shear fracture energy in granite, *Nature*, *350*, 39–42.
Mase, C. W., and L. Smith (1987), Effects of frictional heating on the thermal, hydrologic, and mechanical response of a fault, *J. Geophys. Res.*, *92*, 6249–6272.
Meade, C., and R. Jeanloz (1991), Deep focus earthquakes and recycling of water into the Earth's mantle, *Science*, *252*, 68–72.
Meglis, I. L., P. M. Melanson, and I. J. Jordaan (1999), Microstructural change in ice: II. Creep behavior under triaxial stress conditions, *J. Glaciol.*, *45*, 438–448.
Mitra, S. (1988), Effects of deformation mechanisms on reservoir potential in central Appalachian overthrust belt, *AAPG Bull.*, *72*, 536–554.
Ogawa, M. (1987), Shear instability in a viscoelastic material as the cause for deep focus earthquakes, *J. Geophys. Res.*, *92*, 13,801–13,810.
Orowan, E. (1960), Mechanism of seismic faulting, in *Rock Deformation*, edited by D. T. Griggs and J. Handin, *Mem. Geol. Soc. Am.*, *79*, 323–345.
Perez-Prado, M. T., J. A. Hines, and K. S. Vecchio (2001), Microstructural evolution in adiabatic shear bands in Ta and Ta-W alloys, *Acta Mater.*, *49*, 2905–2917.
Raleigh, C. B., and J. Evernden (1981), Case for low deviatoric stress in the lithosphere, in *Mechanical Behavior of Crustal Rocks*, *Geophys. Monogr. Ser.*, vol. 24, edited by N. L. Carter, pp. 173–186, AGU, Washington, D. C.
Renshaw, C. E., and E. M. Schulson (2001), Universal behaviour in compressive failure of brittle materials, *Nature*, *412*, 897–900.
Rubin, D., and D. C. Drucker (1969), On stability of viscoplastic systems with thermo-mechanical coupling, in *Contributions to Mechanics*, edited by D. Abir, pp. 171–179, Pergamon, New York.
Sanderson, T. J. O. (1988), *Ice Mechanics: Risks to Offshore Structures*, 253 pp., Graham and Trotman, Norwell, Mass.
Schulson, E. M. (2002), Compressive shear faults in ice: Plastic vs. Coulombic faults, *Acta Mater.*, *50*(13), 3415–3424.
Schulson, E. M., and E. T. Gratz (1999), The brittle compressive failure of orthotropic ice under triaxial loading, *Acta Mater.*, *47*, 745–755.
Schulson, E. M., P. N. Lim, and R. W. Lee (1984), A brittle to ductile transition in ice under tension, *Philos. Mag. A*, *49*(3), 353–363.
Shaw, B. E. (1995), Frictional weakening and slip complexity in earthquake faults, *J. Geophys. Res.*, *100*, 18,239–18,251.
Shelton, G. L., J. Tullis, and T. Tullis (1981), Experimental high temperature and high pressure faults, *Geophys. Res. Lett.*, *8*, 55–58.
Shimada, M. (1992), Confirmation of two types of fracture in granite deformed at temperatures to 300°C, *Tectonophysics*, *211*, 259–268.
Shimada, M., and A. Cho (1990), Two types of brittle fracture of silicate rocks under confining pressure and their implications in the Earth's crust, *Tectonophysics*, *175*, 221–235.
Sibson, R. H., and G. Xie (1998), Dip range for intracontinental reverse faults ruptures: Truth not stranger than friction?, *Bull. Seismol. Soc. Am.*, *88*(4), 1014–1022.
Sleep, N. H. (1995), Frictional heating and the stability of rate and state dependent frictional sliding, *Geophys. Res. Lett.*, *22*, 2785–2788.
Thatcher, W., and D. P. Hill (1991), Fault orientations in extensional and conjugate strike-slip environments and their implications, *Geology*, *19*, 1116–1120.
Tullis, J., and R. A. Yund (1977), Experimental deformation of dry Westerly granite, *J. Geophys. Res.*, *82*, 5705–5718.
Tullis, J., and R. Yund (1992), The brittle-ductile transition in feldspar aggregates: An experimental study, in *Fault Mechanics and Transport Properties of Rocks*, edited by B. Evans, pp. 89–117, Academic, San Diego, Calif.
Wiens, D. A. (2001), Seismological constraints on the mechanism of deep earthquakes: Temperature dependence of deep earthquake source properties, *Phys. Earth Planet. Inter.*, *127*, 145–163.
Wilson, C. J. L., Y. Zhang, and K. Stüwe (1996), The effects of localized deformation on melting processess in ice, *Cold Reg. Sci. Technol.*, *24*, 177–189.
Winter, R. E. (1975), Adiabatic shear of titanium and polymethylmethacrylate, *Philos. Mag.*, *31*, 765–773.

C. E. Renshaw, Department of Earth Sciences, 6105 Fairchild, Dartmouth College, Hanover, NH 03755, USA. (carl.e.renshaw@dartmouth.edu)
E. M. Schulson, Thayer School of Engineering, Dartmouth College, Hanover, NH 03755, USA.